

## Effect of Laser Polarization on Photoionization Efficiency of Lutetium

© A.B. D'yachkov, A.A. Gorkunov, A.B. Labozin, S.M. Mironov, V.A. Firsov, G.O. Tsvetkov<sup>¶</sup>, V.Ya. Panchenko

National Research Center "Kurchatov Institute",  
123182 Moscow, Russia

<sup>¶</sup> e-mail: Tsvetkov\_GO@nrcki.ru

Received December 14, 2021

Revised October 28, 2022

Accepted 31.10.2022.

The effect of laser radiation polarization on the photoionization of lutetium is studied using three-stage scheme  $5d6s^2 D_{3/2} - 5d6s6p^4 F_{5/2}^o - 5d6s7s^4 D_{3/2} - (53375 \text{ cm}^{-1})_{1/2}^o$ . It is shown that in a number of cases, there is a limitation of photoionization associated with the features of coherent photoexcitation.

**Keywords:** laser selective photoionization, lutetium-177.

DOI: 10.21883/EOS.2022.12.55237.3034-22

### Introduction

Three-stage photoionization scheme for Lutetium  $5d6s^2 D_{3/2} - 5d6s6p^4 F_{5/2}^o - 5d6s7s^4 D_{3/2} - (53375 \text{ cm}^{-1})_{1/2}^o$  allows photoionization  $^{177}\text{Lu}$  and  $^{177m}\text{Lu}$  with high selectivity and efficiency, which can be used for industrial production of these radionuclides for their medical applications [1]. Lutetium isotopes (except  $^{170}\text{Lu}$ ) have nonzero nuclear spin, so all energy levels are split into multiplets (Fig. 1). The sublevels in the multiplets are determined by the total atomic moment  $F = J + I, J + I - 1, \dots, |J - I|$ , where  $J$  is the total electron moment of the atom,  $I$  is the spin of the nucleus. The difference between the frequencies of excitation of transitions between different components of the hyperfine structure (HFS) ( $\Delta F = 0, \pm 1$ ) turns out, as a rule, to be much larger than the spectral width of laser radiation. Therefore, at a certain setting of laser wavelengths, photoionization occurs only through one channel e.i. combination of the HFS ( $F$ ) components of the ground, first, second excited, and autoionization states. The efficiency of photoionization of each channel is formally limited by the population of the initial component of the ground state.

For example, in the case of photoionization via the 5–6–5–4 channel, the starting component is the component with the total atomic momentum  $F = 5$ . The population of this state, which is proportional to the statistical weight  $2F + 1$ , is 0.34, which, in combination with the temperature population of the ground state, 0.7 (at the evaporation temperature of Lutetium  $1700^\circ\text{C}$ ), gives a limitation on the photoionization efficiency for this channel 0.24. The same constraint holds for any channel whose start state is the main state component, with  $F = 5$  (5–5–4–4, 5–5–5–4, 5–4–4–4 etc This does not mean, however, that all these channels are equivalent in terms of photoionization efficiency. The difference between the absorption frequencies of different isotopes of Lutetium is on the order of 1GHz, and to achieve high selectivity

of photoionization, the use of spectrally narrow lasers is required. In this case, for example, when pulsed single-mode dye lasers with a spectral width of 100–150MHz are used, phenomena are observed that are inherent in the coherent photoexcitation process, when pronounced population oscillations are formed with a Rabi frequency exceeding the natural widths of the transitions under study. In particular, in the work [2] the Autler-Towns effect, which leads to splitting of transition lines, is experimentally studied. The study of the dependence of the splitting on the intensity of laser radiation makes it possible to refine the characteristics of the decay of the levels of the studied scheme of photoionization of Lutetium. Coherent effects in some cases may lead to an additional limitation of the efficiency of photoionization of some channels.

### Calculation

The theoretical analysis of coherent photoionization according to the three-stage scheme is greatly simplified when considering the third stage (autoionization) as a relaxation of the second excited state  $5d6s7s^4 D_{3/2}$ . This approach was successfully applied in the work [3], in our case it allows us to obtain the necessary results without resorting to complex calculations. With this approach, the probability of photoionization turns out to be proportional to the quasi-stationary population of the second excited state, which is formed as a result of the simultaneous action of the laser radiation of the first and second stages on the atom. Such problems were theoretically considered in the works [4–7]. The probability, averaged over Rabi oscillations, of finding an atom in the second excited state is described [5] by the formula

$$W_2 = \frac{3}{2} \frac{\Omega_1^2 \Omega_2^2}{(\Omega_1^2 + \Omega_2^2)^2}, \quad (1)$$

where  $\Omega_1$  and  $\Omega_2$  are the Rabi frequencies at the first and second transitions. In order to determine the Rabi frequency taking into account the STS, the formula

$$\hbar\Omega = |\mathbf{d}_{F\neq} \mathbf{E}_0|, \quad (2)$$

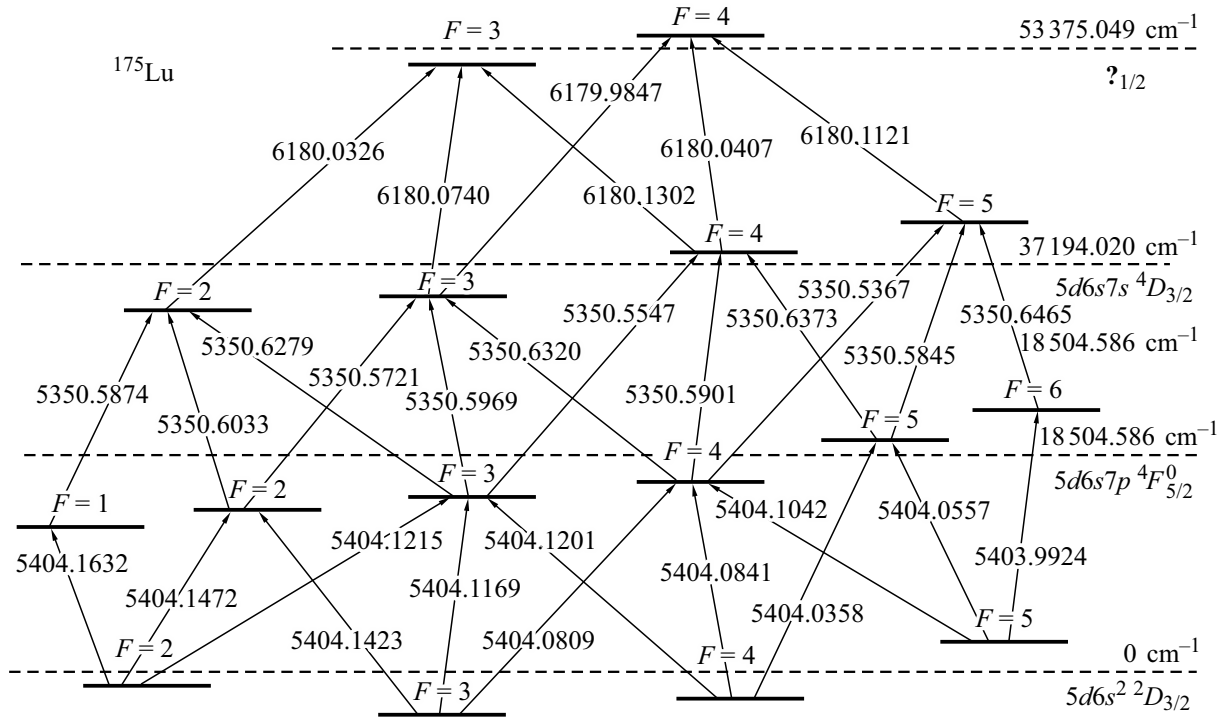


Figure 1. Lutetium photoionization scheme  $^{175}\text{Lu}$ .

where  $\mathbf{d}_{F\hat{F}}$  is the dipole moment vector operator of the transition from the state with the quantum number of the total mechanical moment  $\hat{F}$  to the state  $F$ , and  $\mathbf{E}_0$  is the amplitude vector of the electric field of the electromagnetic wave of laser radiation. Matrix element of the transition dipole moment  $d_{F\hat{F}}$  between hyperfine structure states with quantum numbers  $I, J, F, M \rightarrow I, \hat{J}, \hat{F}, \hat{M}$  is expressed [7] in terms of the reduced matrix element  $\langle J \parallel D \parallel \hat{J} \rangle$  by the formula

$$d_{F\hat{F}} = (-1)^{F-M} \begin{pmatrix} F & 1 & \hat{F} \\ -M & q & \hat{M} \end{pmatrix} (-1)^{I+J+F+1} \times \sqrt{(2F+1)(2\hat{F}+1)} \begin{Bmatrix} J & 1 & \hat{J} \\ \hat{F} & I & F \end{Bmatrix} \langle J \parallel D \parallel \hat{J} \rangle, \quad (3)$$

where  $F$  and  $\hat{F}$  are quantum numbers of the total mechanical momentum of the atom (nucleus and electrons),  $\hat{M}$  and  $M$  are their projections,  $\hat{J}$  and  $J$  are quantum numbers of the total orbital and spin momentum of electrons,  $I$  is nuclear spin,  $q$  is polarization parameter of laser radiation ( $q = 0$  for linear polarization and  $q = \pm 1$  for circular polarization).

The elements  $\begin{pmatrix} F & 1 & \hat{F} \\ -M & q & \hat{M} \end{pmatrix}$  and  $\begin{Bmatrix} J & 1 & \hat{J} \\ \hat{F} & I & F \end{Bmatrix}$  are the  $3j$ - and  $6j$ -Wigner symbols, respectively [9,10]. In turn, the reduced dipole moment  $\langle J \parallel D \parallel \hat{J} \rangle$  is expressed [7,11] in terms of the transition characteristics:

$$|\langle J \parallel D \parallel \hat{J} \rangle|^2 = \frac{3\hbar\lambda^3(2\hat{J}+1)}{4 \cdot 8\pi^3} A(\hat{J} \rightarrow J), \quad (4)$$

where  $A(\hat{J} \rightarrow J)$  is the Einstein coefficient of the corresponding transition.

Thus, for channel 5–6–5–4, the Rabi frequencies are expressed as follows:

$$\Omega_1 = \begin{pmatrix} F & 1 & \hat{F} \\ -M & q & \hat{M} \end{pmatrix} \sqrt{143} \sqrt{\frac{1}{66}} \sqrt{\frac{3\lambda^3 I A_1(5/2 \rightarrow 3/2)}{\hbar\pi^2 c}}, \quad (5)$$

$$\Omega_2 = \begin{pmatrix} F & 1 & \hat{F} \\ -M & q & \hat{M} \end{pmatrix} \sqrt{143} \sqrt{\frac{1}{66}} \sqrt{\frac{3\lambda^3 I A_2(3/2 \rightarrow 5/2)}{\hbar\pi^2 c}}. \quad (6)$$

Similarly for channel 5–5–5–4

$$\Omega_1 = \begin{pmatrix} F & 1 & \hat{F} \\ -M & q & \hat{M} \end{pmatrix} \frac{11}{5} \sqrt{\frac{7}{66}} \sqrt{\frac{3\lambda^3 I A_1(5/2 \rightarrow 3/2)}{\hbar\pi^2 c}}, \quad (7)$$

$$\Omega_2 = \begin{pmatrix} F & 1 & \hat{F} \\ -M & q & \hat{M} \end{pmatrix} \frac{11}{5} \sqrt{\frac{7}{66}} \sqrt{\frac{3\lambda^3 I A_2(3/2 \rightarrow 5/2)}{\hbar\pi^2 c}}. \quad (8)$$

For linear polarization of laser radiation ( $\Delta M = 0$ ), the absolute values of  $3j$ -symbols are shown in the diagram (Fig. 2) for channels 5–6–5–4 and 5–5–5–4.

It follows from formula (1) that the maximum value of  $W_2 = 3/8$  is achieved at equal Rabi frequencies:

$$\Omega_1 = \Omega_2. \quad (9)$$

The dependences of  $W_2$  on the intensity of laser radiation at the second stage for channels 5–6–5–4 and 5–5–5–4 are shown in Fig. 3.

In contrast to incoherent photoionization, the coherent population first increases with increasing intensity, reaching

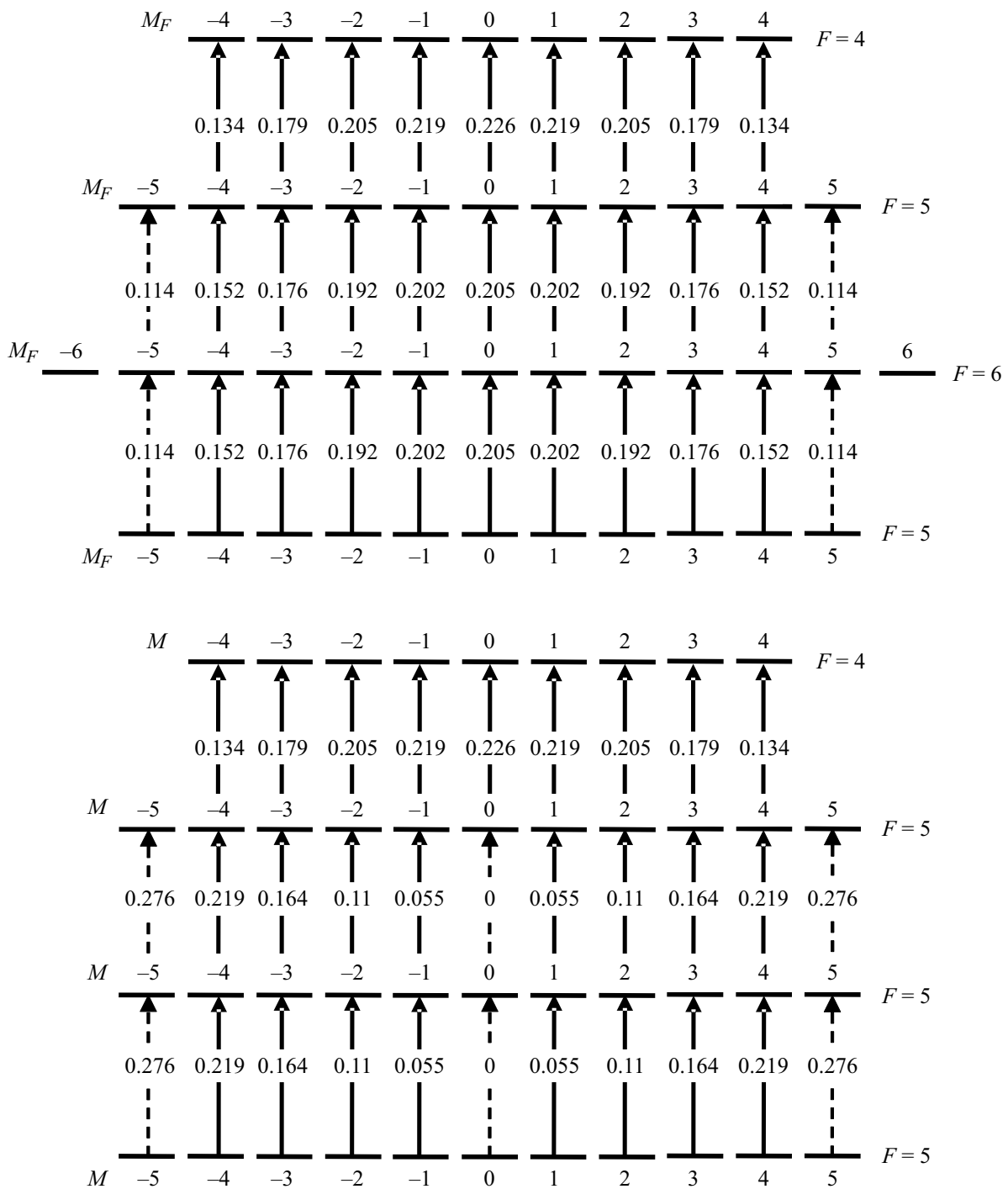


**Figure 2.** Transition projection schemes and absolute values of 3j-symbols for channels 5-6-5-4 (top) and 5-5-5-4 (bottom). Linear polarization.

a maximum when the Rabi frequencies are equal. As the intensity increases further, the coherent population decreases and tends to zero, while the incoherent one remains constant. Due to the fact that the ratios of the 3j-symbols at the first and second transitions are the same, the intensity dependences constructed by formula (1) for different projections coincide. To estimate the efficiency of photoionization, the figure also shows the populations of the

second excited state averaged over 11 projections:

$$\bar{W}_2 = \left[ W_2(M = 0) + 2W_2(M = 1) + 2W_2(M = 2) + 2W_2(M = 3) + 2W_2(M = 4) \right] / 11. \quad (10)$$

The maximum of averaged population for channel 5-5-5-4 turns out to be less than for channel 5-6-5-4, due to the fact

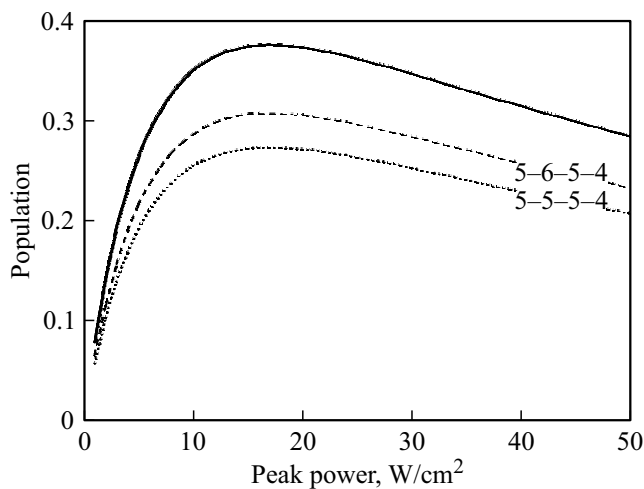


**Figure 3.** Linear polarization. Dependence of the population of the second excited state on the intensity of the laser radiation of the second stage (solid curve). Averaged population of the second excited state in channels 5-6-5-4 (dotted curve) and 5-5-5-4 (pointed line). The intensity of the first stage is 150 W/cm<sup>2</sup>.

that the transition between the projections M 0→0→0→0 for channel 5-5-5-4 is disabled.

Schemes of transition projections and absolute values of 3j-symbols for circular polarization ( $q = -1$ ) are shown in the diagram (Fig. 4). Figure 5 shows the dependence of the populations  $W_2$  for circular polarization for various projections of the initial state on the channel 5-6-5-4. It can be seen from the figure that, in the case of circular polarization, the ratios of the 3j symbols at the first and second transitions differ significantly for different starting projections. Correspondingly, the positions of the population maxima for various combinations of projections associated with circular polarization also differ. In this connection, it is impossible to choose the intensities of the laser radiation of the first and second stages in such a way that photoionization from all starting projections can be equally effective. For example, for a combination of projections 5→4→3→2, the intensity of the second stage 10 W/cm<sup>2</sup> turns out to be too high, and it almost does not work (the population is below 0.05), as well as for the combination 4→3→2→1 (the population is less than 0.15). Projection combinations 3→2→1→0, 2→1→0→1, 1→0→1→2 and 0→1→2→3 are close to the maximum, and for the combination -1→2→-3→-4 the intensity is insufficient (population below 0.15). As a result, the average population does not rise above 0.15.

The situation with circular polarization in the 5-5-5-4 channel is much better (Fig. 4). The maxima of different combinations of the projection turn out to be much closer to each other, which is responsible for the higher (~0.235) averaged population of the second excited state (Fig. 6).

For comparison, Fig. 7 shows the averaged populations for linear and circular polarizations on channels 5-6-5-4 and 5-5-5-4. The most efficient photoionization occurs with linear polarization on the 5-6-5-4 channel, linear

polarization on the 5-5-5-4 channel is slightly inferior to it due to the forbidden combination projections 0→0→0→0. Circular polarization noticeably loses to linear polarization due to the inhomogeneity of the ratios of the transition forces of the first and second steps.

## Experiment

The effect of polarization on the photoionization efficiency <sup>175</sup>Lu was studied using the  $5d6s^2\ ^2D_{3/2} - 5d6s6p\ ^4F_{5/2}^o - 5d6s7s\ ^4D_{3/2} - (53375\text{ cm}^{-1})_{1/2}^o$  by laser resonance ionization mass spectroscopy (LRIMS). For resonant excitation and ionization of atoms, radiation from three pulsed dye lasers (DLs) (540, 535, and 618 nm) was used, pumped by a copper vapor laser with a pulse repetition rate of 10 kHz. Each DL consisted of a master oscillator operating on one longitudinal mode in the mode of active wavelength stabilization, and a DL amplifier. The output average powers of the DLs were 1–4 W, the spectral width of the generation line was 100–150 MHz (FWHM), and the pulse duration was 15 ns (FWHM).

The beams of three DLs were telescoped to the size  $\varnothing = 10\text{ mm}$  and collimated. Their spatial convergence was carried out on translucent and dichroic mirrors. A system of rotating mirrors directed a single three-color beam to the mass spectrometer (MS) chamber. Due to the design features of the laser system, the radiation of three DLs was linearly polarized in a single plane.

Photoions were detected using a commercial MS-7302 quadrupole mass spectrometer. An atomic beam with a divergence angle  $\sim 3^\circ$  was formed by the evaporation of metallic lutetium in high vacuum at a temperature  $\sim 2000^\circ\text{C}$ , the Doppler broadening of atoms in the beam  $\sim 150\text{ MHz}$ . The average thermal velocity of atoms in the beam was about 550 m/s. Therefore, for a laser pulse duration of 15 ns, the region of interaction of laser radiation with an ensemble of atoms 2 mm in diameter can be considered an isolated system, neglecting the time-of-flight broadening. The density of atoms in the interaction region was about  $10^{10}\text{ cm}^{-3}$  and the residual gas pressure  $(1-2) \cdot 10^{-6}\text{ Torr}$ , which virtually eliminates collisions of beam atoms both with each other and with molecules of the residual gas. The technical parameters and features of the experimental unit are described in detail in the works [12,13].

To change the polarization of the laser radiation (linear ↔ circular), a quarter-wave plate made of 10mm thick quartz glass was used. Optical anisotropy was created by uniaxial compression across the laser beam axis. The pressure was set until the phase shift of  $\pi/2$  at the wavelength of 540 nm was reached at the output of the plate (first stage). Due to the proximity of the wavelengths, the transition to circular polarization was carried out simultaneously for the beam of the second stage 535 nm. The ellipticity of the radiation polarization 618 nm (third step) was 0.8.

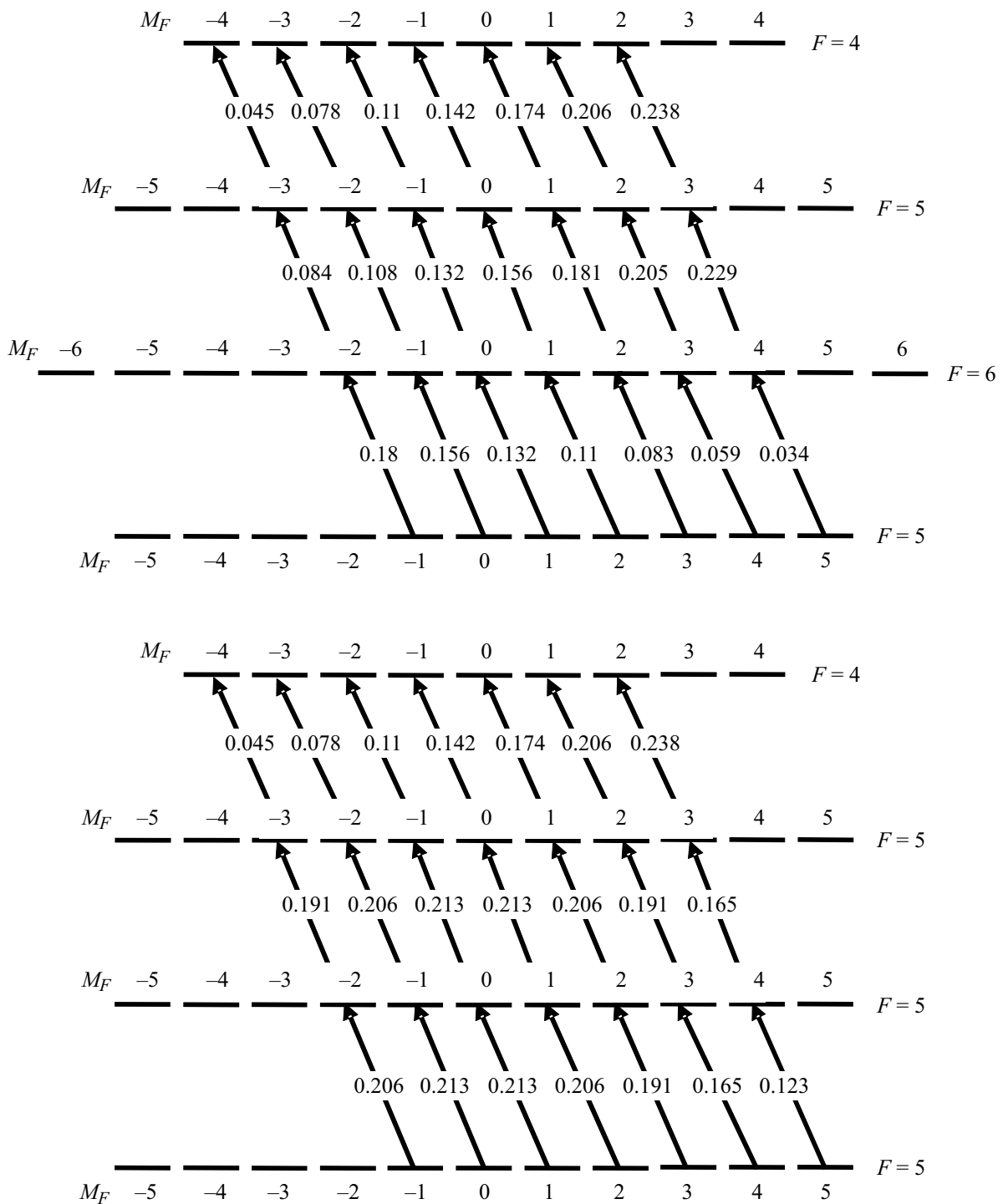


**Figure 4.** Scheme of projection of transitions for circular polarization ( $q = -1$ ) and absolute values of  $3j$ -symbols for channels 5-6-5-4 (top) and 5-5-5-4 (bottom).

### Results and discussion

Fig. 8 shows a recording of the photoion signal <sup>175</sup>Lu when the polarization of laser radiation is changed from linear to circular for channels 5-6-5-4 and 5-5-5-4. The regions when the photoion signal decreases to zero correspond to the laser beams stopping periods of laser

beams in the process of changing their polarizations by 45° rotation of the quarter-wave plate. Results are summarized in the table.

It can be seen from the table that the ratios of the experimentally measured values of the photoion current are in good agreement with the average population of the

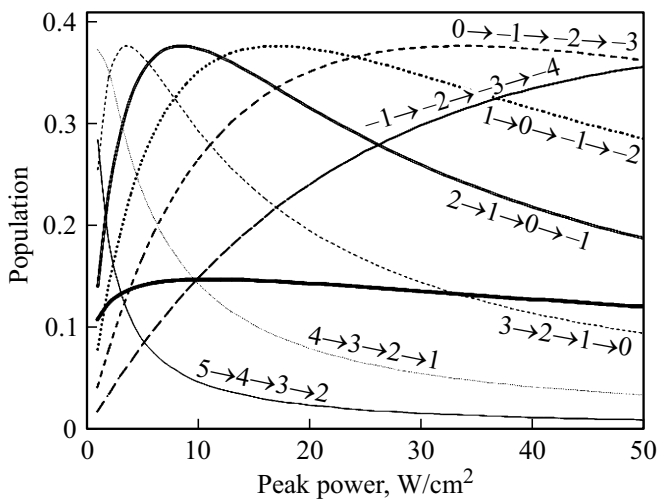


**Figure 5.** Circular polarization ( $q = -1$ ), photoionization channel 5-6-5-4. Dependence of the population of the second excited state on the intensity of the laser radiation of the second stage for different projections. The wide thick line is the average population. The intensity of the first stage is  $150 \text{ W/cm}^2$ .

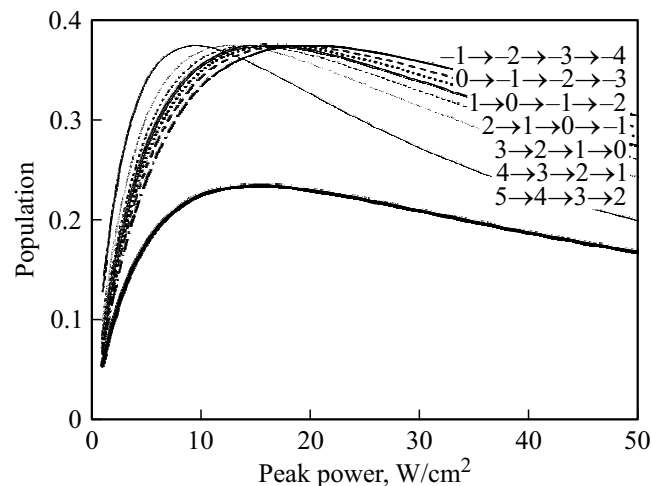


**Figure 6.** Circular polarization ( $q = -1$ ), photoionization channel 5-5-5-4. Dependence of the population of the second excited state on the intensity of the laser radiation of the second stage for different projections. The wide thick line is the average population. The intensity of the first stage is  $150 \text{ W/cm}^2$ .

second excited state calculated by formulas (1)–(9). It should be noted that the incoherent approach based on determining the rate of each transition separately does not allow one to obtain results consistent with experiment. It is the application of the coherent approach, which takes into account the interference of the population fluctuations of the levels of the first and second transitions for each combination of projections with the subsequent summation of the results, that made it possible to achieve agreement with the experimental data.

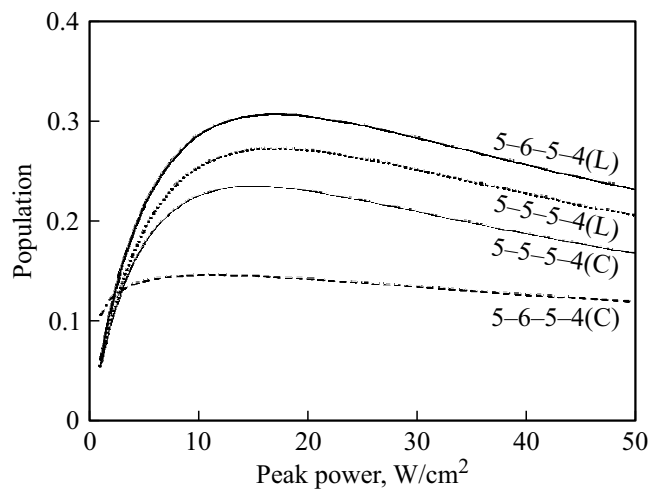


**Figure 7.** Dependence of the averaged population of the second excited state on the intensity of laser radiation at the second stage for the channels 5-6-5-4 and 5-5-5-4 in the case of a linear (L) and circular (C) polarizations. The intensity of the first stage is  $150 \text{ W/cm}^2$ .

**Table**

Channel jf photoionization	Polarization	Photoionic signal (experiment), arb. units	Population (calculation)
5-6-5-4	linear	$31 \pm 3$	0.31
	circular	$13 \pm 1$	0.14
5-5-5-4	linear	$29 \pm 3$	0.27
	circular	$23 \pm 2$	0.23

### Conclusion

When pulsed narrow-band single-mode laser radiation is used, a coherent photoexcitation pattern may arise, which in some cases limits the efficiency of multistage photoionization. Such cases include the situation when the ratios of the transition forces in neighboring photoionization steps are very different for different projections of the initial state, and no combination of intensities can satisfy the condition of equal Rabi frequencies for all combinations of the projection of states. The results of the study speak in favor of the fact that during the laser pulse, various combinations of projections behave as isolated systems, and the more precisely the condition of equality of Rabi frequencies for neighboring steps for each projection is met, the more efficiently photoionization proceeds throughout the channel.

### Funding

The study was supported by a grant from the Russian Science Foundation (Project № 17-13-01180).

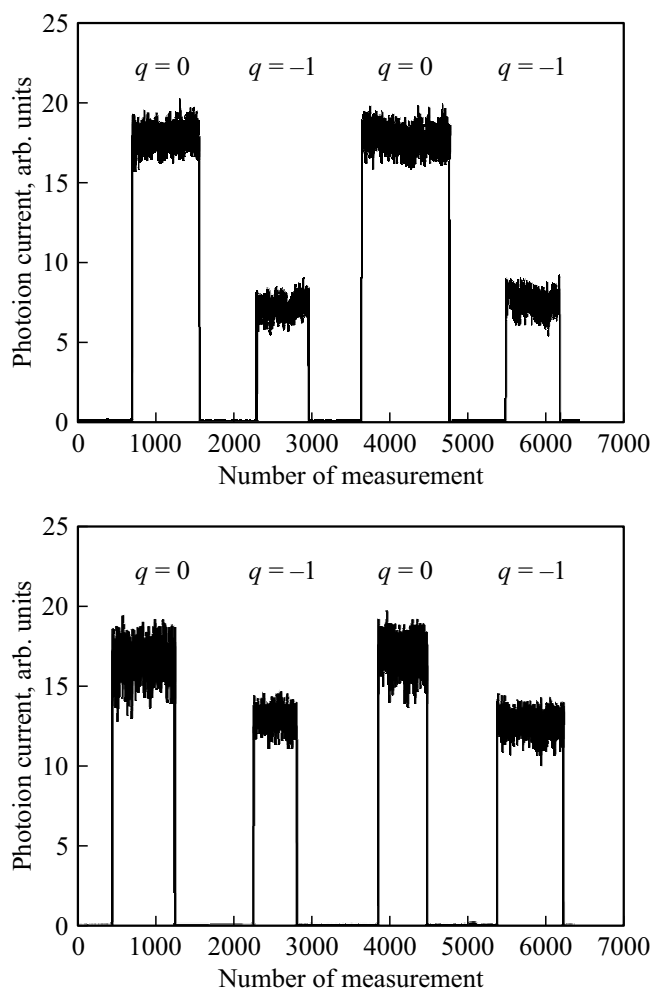


**Figure 8.** Recording of a photoion signal  $^{175}\text{Lu}$  in photoionization channels 5–6–5–4 (top) and 5–5–5–4 (bottom) with a simultaneous change in the polarization of the LC on all steps  $q = 0 \rightarrow -1 \rightarrow 0 \rightarrow -1$ . The signal dips to zero correspond to the laser beams stopping periods of the laser beams to change the polarization of the beams by  $45^\circ$ -turning the quarter-wave plate. The intensity of the DC of the first and second stages is 150 and  $20 \text{ W/cm}^2$ , respectively.

### Conflict of interest

The authors declare that they have no conflict of interest.

### References

- [1] A.B. Dyachkov, A.A. Gorkunov, A.V. Labozin, K.A. Makoveeva, S.M. Mironov, V.Y. Panchenko, V.A. Firsov, G.O. Tsvetkov. *Opt. Spectrosc.*, **128**, 6–11 (2020). DOI:10.1134/S0030400X20010087
- [2] A.B. Dyachkov, A.A. Gorkunov, A.V. Labozin, S.M. Mironov, V.A. Firsov, G.O. Tsvetkov, V.Ya. Panchenko. *Kvant. elektron.*, **4** (367), 370 (2022) (in Russian). [http://www.mathnet.ru/php/archive.phtml?wshow=paper&jrnid=qe&paperid=18029&option\\_lang=rus](http://www.mathnet.ru/php/archive.phtml?wshow=paper&jrnid=qe&paperid=18029&option_lang=rus).
- [3] M.V. Suryanarayana. *JOSA B*, **38**, 353–370 (2021).
- [4] B.W. Shore, J. Ackerhalt. *Phys. Rev. A*, **15**, 1640–1647 (1977). DOI: 10.1103/PhysRevA.15.1640
- [5] Z. Białynicka-Birula, I. Białynicki-Birula, J.H. Eberly, B.W. Shore. *Phys. Rev. A*, **16**, 2048–2054 (1977). DOI: 10.1103/PhysRevA.16.2048
- [6] B.W. Shore. *Phys. Rev. A*, **23**, 1608–1610 (1981). DOI: 10.1103/PhysRevA.23.1608
- [7] B. Shore. *Acta Phys. Slovaca. Rev. Tutorials*, **58**, 243–486 (2008).
- [8] J.H. Eberly, B.W. Shore, Z. Białynicka-Birula, I. Białynicki-Birula. *Phys. Rev. A*, **16**, 2038 (1977).
- [9] I.I. Sobel'man. *Introduction to the Theory of Atomic Spectra* (International Series of Monographs in Natural Philosophy, Elsevier, 2016).
- [10] O. Axner, J.O. Gustafsson, N. Omenetto, J.D. Winefordner. *Spectrochim. Acta B*, **59**, 1–39 (2004). DOI: 10.1016/j.sab.2003.10.002
- [11] V.B. Berestetskiy. *Relyativistskaya kvantovaya teoriya* (Nauka, 1968) (in Russian).
- [12] A.B. D'yachkov, A.A. Gorkunov, A.V. Labozin, S.M. Mironov, V.Y. Panchenko, V.A. Firsov, G.O. Tsvetkov. *Quant. Electron.*, **48**, 75–81 (2018). DOI: 10.1070/qel16493
- [13] A.B. D'yachkov, A.A. Gorkunov, A.V. Labozin, S.M. Mironov, V.Y. Panchenko, V.A. Firsov, G.O. Tsvetkov. *Instruments Exp. Tech.*, **61**, 548–555 (2018). DOI: 10.1134/S0020441218040048